An easy method for the evaluation of visual tumor heterogeneity of ^{18}F-FDG PET/CT using 10-step color scale: A correlative study in patients with lung cancer

Bum Soo Kim[1] **MD,**
Heeyoung Kim[1] **MD,**
Sungmin Jun[1] **MD, PhD**

1. Department of Nuclear Medicine, Kosin University Gospel Hospital, Kosin University College of Medicine, Busan, Korea

Keywords: Peritumoral halo layer - Lung cancer - ^{18}F-FDG -PET - Texture analysis

Corresponding author:
Sungmin Jun MD, PhD,
Department of Nuclear Medicine,
Kosin University Gospel Hospital,
Kosin University College of Medicine, Busan, Korea
Tel; 82-51-990-6661
Fax; 82-51-990-3600
fanace@daum.net

Received:
29 June 2020
Accepted revised:
24 July 2020

Abstract

Objectives: The purpose of this study was to assess the correlation between visual assessment by the peritumoral halo layer (PHL) method and analysis with texture and intensity histogram metrics for evaluating tumor heterogeneity (TH) in fluorine-18-fluorodeoxyglucose (^{18}F-FDG) positron emission tomography/computed tomography (PET/CT) of patients with lung cancer. **Subjects and Methods:** We retrospectively reviewed the 64 patients with records of ^{18}F-FDG PET/CT prior to treatment. After tumor segmentation by the PHL method, three visual patterns: the existence of cold defect, the location of hottest core, and number of irregular layers can be obtained on ^{18}F-FDG PET/CT images. To examine the correlation, first-order entropy was extracted by texture analysis and the area under curve-cumulative SUV-volume histogram (AUC-CSH) value was used in the intensity histogram analysis. A correlation between the visual assessment and the parameters of the metrics analysis was evaluated. We also evaluated the inter-correlation among the visual assessment and correlation between metabolic tumor volume (MTV) and parameters of TH. **Results:** A significant correlation was noted between visual assessment and quantitative indices of texture and intensity histogram analysis with high inter-observer agreement. Additionally, a significant inter-correlation between the existence of cold defect, location of hottest core, and the number of irregular layers was observed. Metabolic tumor volume was correlated with all of the parameters in the ^{18}F-FDG PET/CT images, such as AUC-CSH, entropy, existence of cold defect, location of hottest core, and number of irregular layers. **Conclusions:** In this study, we provide a new visual assessment criterion of TH with a strong inter-observer agreement. The visual analysis using the PHL method could be a potential marker for evaluating heterogeneous tumors.

Hell J Nucl Med 2020; 23(2): 158-164 *Epub ahead of print: 27 July 2020* *Published online: 24 August 2020*

Introduction

Fluorine-18-fluorodeoxyglucose (^{18}F-FDG) positron emission tomography/computed tomography (PET/CT) is an important, non-invasive assessment tool in clinical practice, especially in the cancer field. Fluorine-18-FDG PET/CT can provide a range of standard parameters, such as standard uptake value (SUV), metabolic tumor volume (MTV), and total lesion glycolysis (TLG). However, the standard parameters are limited in describing accurate tumor characteristics [1]. Tumor heterogeneity (TH) is a well-known characteristic of tumors that illustrates the intratumoral phenotypical and functional differences among cancer cells that occur during disease progression [2]. Recent studies have shown that TH could be measured using ^{18}F-FDG PET/CT to provide useful clinical information regarding response to treatment, survival, and differentiation of tumor types because it reflects underlying biology such as hypoxia, proliferation, necrosis, and vascularization of the tumor [2-5]. Tumor heterogeneity assessment on ^{18}F-FDG PET/CT can be analyzed with various methods. The most commonly used is the texture analysis and intensity histogram analysis, which are the most extensively studied. Assessment based on texture and intensity histogram analyses could be used to quantify the properties of tumors and provide useful clinical information for various cancer models [3, 6, 7].

Recent studies have shown a significant correlation between TH by visual assessment and TH by quantitative metrics including texture analysis and intensity histogram in ^{18}F-FDG PET/CT [8, 9]. The results suggest that visual assessment could be a reliable method for assessing TH. Previous studies have used a visual scoring system [8-10]. The visual evaluation may cause confusion when analyzing images because in a visual scoring system, each grade may not be distinctly differentiated, which could lead to an inter-observer disagreement.

Jun et al. (2018) introduced new method for tumor segmentation, a distinct layer named peritumoral halo layer (PHL) between the tumor and background activity in 10-step color scale with specific window level settings [11, 12]. They also proposed that TH can be visually assessed using the PHL method. Three visual patterns were suggested in case of heterogeneous tumor: the existence of cold defect, the location of hottest core (center or eccentric portion), and number of irregular layers [11].

Here, we investigated the possible correlation between visual assessment of TH by the new tumor segment method (PHL method) and other metrics of TH (texture and intensity histogram analyses) to determine whether visual assessment using the PHL method could be used to study TH non-invasively.

Subjects and Methods

Subjects

Between July 2019 and December 2019, 107 consecutive patients with lung cancer with records of ^{18}F-FDG PET/CT scans prior to treatment were initially included in this study. Of the 107 patients, 43 patients were excluded for the following criteria: (1) Conglomerated hypermetabolic lymph nodes adjacent to the main tumor (n=19). (2) Hypermetabolic post-obstructive pneumonia surrounding the main tumor (n=11). (3) Non-^{18}F-FDG-avid primary tumor (n=7). (4) Hypermetabolic pleural metastasis closely adjacent to the main tumor (n=3). (5) Fluorine-18-FDG-avid metastatic nodules near the main tumor (n=2), and (6) intense physiologic cardiac uptake adjacent to the main tumor (n=1). A total of 64 patients were finally included in the study. This retrospective study was approved by our institutional review board and performed in accordance with the tenets of the Declaration of Helsinki.

^{18}F-FDG PET/CT

Patients fasted for at least 6 hours before ^{18}F-FDG injection (370- 444MBq). Serum glucose level was measured before ^{18}F-FDG injection. The scan was performed 50-70min after injection of ^{18}F-FDG using a Siemens Biograph mCT-64 PET/CT scanner (Siemens Healthcare, Knoxville, TN, USA). Patients were asked to rest before acquisition of PET/CT images. Before the PET scan, a non-contrast low-dose CT scan (3mm slices) was obtained for attenuation correction and anatomic co-registration. Images were obtained from the skull base to the proximal thigh with the patient in the supine position. Positron emission tomography images were acquired using an acquisition time of 3min per table position in 3-dimensional mode with an acquisition of 90 seconds per bed position. The PET images were reconstructed iteratively using ordered subset expectation maximization. Positron emission tomography images were corrected for attenuation using a CT-derived transmission map. The voxel size after reconstruction was 4.07mm×4.07mm×3.0mm.

Tumor segmentation by the PHL method

The tumor segmentation method of PHL was performed as previously published [11, 12]. Briefly, (1) the PET contrast window level was set in SUV units; (2) the top value of the window level was set slightly higher than the SUVmax of lung cancer, and the bottom value was set to zero; (3) the color scale was set to 10-step color scale; (4) the PHL was identified by an abrupt increase in layer thickness with minimal distortion of the tumor contour between the tumor and background activity; and (5) the tumor threshold was defined as the layer just inside the PHL because the PHL layer is always located between the tumor and background activity.

Analysis of tumor heterogeneity

After the aforementioned tumor segmentation, visual assessment of TH was evaluated based on 3 patterns: (1) The presence of cold defect. (2) Whether the hottest core is located at the center or periphery (or eccentric), and (3) the number of layers with irregular margin that are visible (Figure 1). A previous study reported that cold defects were observed relatively frequently, the hottest core was located in an eccentric portion of the tumor, and multiple irregular layers were found in the heterogeneous tumor. On the contrary, there could be no cold defect, the hottest core is located in the center of the tumor, or very few or no irregular layers are detected in the homogenous tumor [11].

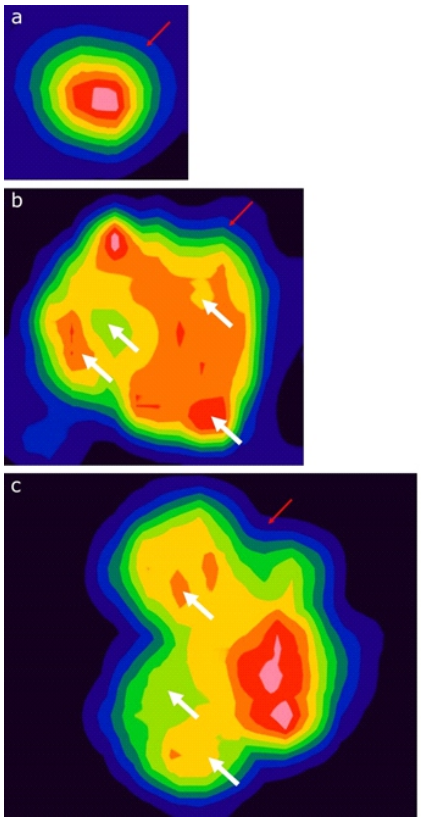

Figure 1. Representative tumors for three visual patterns. a) Visually homogenous tumor. The cold defect is not visible, and central hottest core can be confirmed. Regular margins are observed in all tumor layers. The PHL layer (red arrow, 20% of SUVmax) is located between tumor and background activity. b) Visually heterogeneous tumor. The cold defect is observed, and the hottest core is located in the eccentric portion. Four irregular layers (white arrow) are visually observed. The PHL layer is located in 20% of SUVmax (red arrow). c) Visually heterogeneous tumor. Cold defect is not visible, and the hottest core is in peripheral. Three irregular layers (white arrow) are observed, and the PHL layer is located in 10% of SUVmax (red arrow).

We also examined conventional parameters such as maximum SUV (SUVmax) and MTV in the primary tumors. The MTV, as a metabolic-volumetric parameter, was determined with the tumor threshold via the PHL method in the study. Visual assessment, semi-quantitative (SUVmax), and quantitative (MTV) measurements were analyzed on workstation (Siemens Syngo.via, Siemens Healthcare, Erlangen, Germany).

The area under curve-cumulative SUV-volume histogram (AUC-CSH) method is used in measuring TH by intensity histogram analysis [7, 8, 13]. The AUC-CSH value was calculated as the area under the curve (AUC) of a cumulative SUV-volume histogram (CSH) obtained by plotting the percent volume greater than a certain threshold of the SUVmax. In this study, the threshold of SUVmax lies between the tumor threshold by PHL method and 100% of SUVmax (e.g., if the tumor threshold by PHL method was 30%, the threshold of SUVmax values was set between 30% to 100%). The threshold of the SUVmax value increased every 10%. Area under curve-cumulative SUV-volume histogram is a quantitative index of uptake heterogeneity where lower values correspond to increased heterogeneity.

Feature extraction via texture analysis was performed using LIFEx (IMIV, CEA, France). Volume of interest (VOI) was drawn over the tumor in the lung. First-order entropy was extracted based on the VOI. Tumor segmentation was determined using a fixed threshold of the SUV value, which was 2.5 ($Entropy_{2.5}$), and a tumor threshold by the PHL method ($Entropy_{PHL}$). Voxel values within the tumor VOI were resampled to yield 64 grey bins. Entropy describes the randomness of gray-level voxel intensities within an image and was determined using the following formula:

$$\text{Entropy} = -\sum_{i} p(i) \cdot \log(p(i) + \varepsilon)$$

where p(i) is the probability of occurrence of voxels with an intensity i and $\varepsilon = 2e\text{-}16$.

Statistical analysis

To investigate any relationship between visual patterns of PHL method (existence of cold defect and location of hottest core) and other metrics of TH (texture and intensity histogram analysis), the Mann-Whitney test was used. The Kruskal-Wallis test was used to compare the differences in AUC-CSH and entropy values according to the number of irregular layers. Weighted kappa statistics were performed to evaluate the inter-observer agreement between the two nuclear medicine physicians for PHL threshold, existence of cold defect, location of hottest core, and the number of irregular layers. Levels of agreement were quantified using weighted κ (κ_w), and κ_w was interpreted according to the criteria set by Landis and Koch. To analyze the possibility of inter-correlation among the visual assessment, Mann-Whitney and Fisher's exact tests were used. All statistical analyses were performed on MedCalc software (MedCalc, Mariakerke, Belgium).

Results

Patient characteristics

A total of 64 patients were finally included in the study. The patient demographics and characteristics are summarized in Table 1. The median age of the patients at the time of the ^{18}F-FDG PET/CT scan was 69.5 years (range, 50-87 years). The study population included patients with adenocarcinoma (n=38, 59.3%), squamous cell carcinoma (n=20, 31.2%), and small cell lung cancer (n=6, 9.3%). Disease stage was based on the 8th edition of the American Joint Committee on Cancer tumor, node, metastasis (TNM) staging manual. There were 18 (28.1%), 8 (12.5%), 24 (37.5%), and 14 (21.8%) patients with TNM stages I, II, III, and IV cancer.

Table 1. *Patient characteristics.*

Characteristic	n (%)
Gender	
Male	43 (67.2)
Female	21 (32.8)
Age	
>65	42 (65.6)
≤65	22 (34.4)
Histology	
Adenocarcinoma	38 (59.4)
Squamous cell carcinoma	20 (31.2)
Small cell lung cancer	6 (9.4)
T	
T1	26 (40.6)
T2	19 (29.7)
T3	8 (12.5)
T4	11 (17.2)
N	
N0	27 (42.2)
N1	7 (10.9)
N2	17 (26.6)
N3	13 (20.3)
Stages	
IA	12 (18.8)
IB	6 (9.4)
IIA	3 (4.7)
IIB	5 (7.8)
IIIA	15 (23.4)
IIIB	8 (12.5)
IIIC	1 (1.6)
IV	14 (21.9)

Inter-observer agreement test

Two observers evaluated all 64 patients and assigned a PHL tumor threshold and three visual patterns for TH to each patient. There was a strong inter-observer agreement for the PHL threshold (κ_w=0.883), the existence of cold defect (κ_w=0.938), the location of the hottest core (κ_w=0.937), and number of irregular layers (κ_w=0.908).

Correlation between visual assessment and quantitative indices of texture and intensity histogram analysis

Area under curve-cumulative SUV-volume histogram (P=0.0047) and $Entropy_{2.5}$ (P=0.0215) values were significantly

different according to the existence of cold defect in Mann-Whitney test. While a trend was demonstrated with Entropy$_{PHL}$ (P=0.0911) (Figure 2). The AUC-CSH (P=0.0218), Entropy$_{PHL}$ (P=0.0004), and Entropy$_{2.5}$ (P<0.0001) values differed significantly between central hottest core and peripheral hottest core in the tumors (Figure 3). When we evaluated the number of irregular layers using the Kruskal-Wallis test, the AUC-CSH (P=0.0026), Entropy$_{PHL}$ (P<0.0001), and Entropy$_{2.5}$ (P<0.0001) values were significantly different among the number of layers (Table 2) (Figure 4).

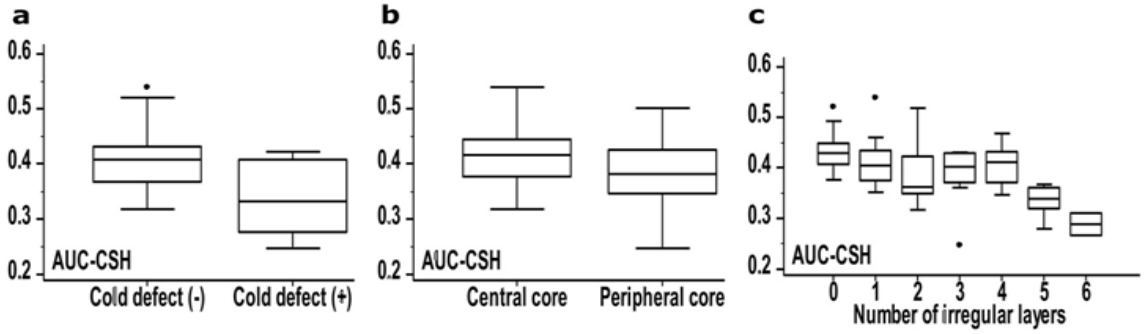

Figure 2. Comparison graphs demonstrated the distribution of AUC-SCH values according to the three visual patterns. a) Mann-Whitney test shows that AUC-CSH values was significantly higher (low heterogeneity) in tumors without cold defect than tumors with cold defect (P=0.004). b) Mann-Whitney test represents that AUC-CSH values was significantly higher (low heterogeneity) in tumors with core in center than tumors with core in peripheral (P=0.021). c) Kruskal-Wallis test shows AUC-CSH values were significantly different among the number of irregular layers. The highest AUC-CSH values (low heterogeneity) were observed tumors without irregular layers. The lowest AUC-CSH values (high heterogeneity) was observed in tumors with 6 irregular layers (P=0.002).

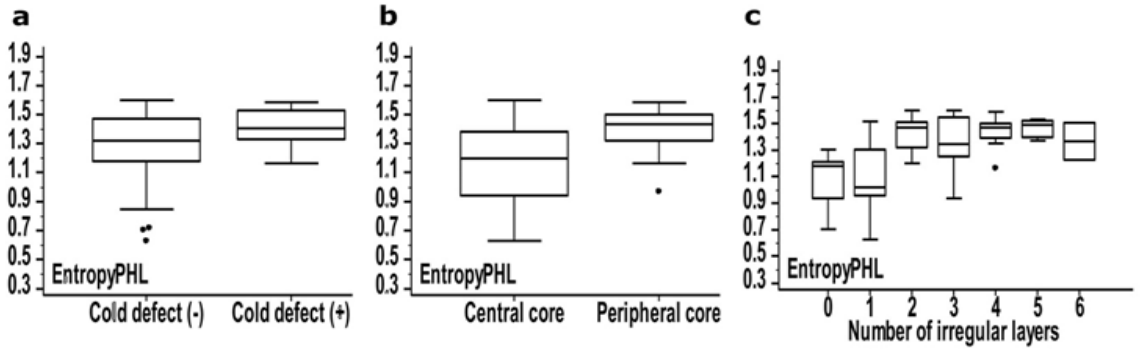

Figure 3. Comparison graphs demonstrated the distribution of Entropy$_{PHL}$ values according to the three visual patterns. a) Mann-Whitney test shows a week association between the existence of cold defect and Entropy$_{PHL}$ (P=0.091). b) The location of hottest core (P<0.001) and c the number of irregular layers (P<0.001) are statistically significant.

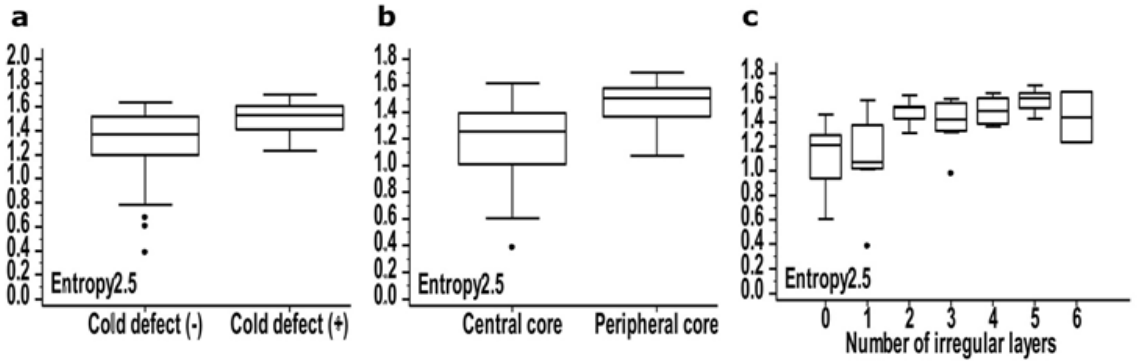

Figure 4. Comparison graphs demonstrated the distribution of Entropy$_{2.5}$ values according to the three visual patterns. a) Mann-Whitney test shows that Entropy$_{2.5}$ values was significantly higher (high heterogeneity) in tumors with cold defects than tumors without cold defect (P=0.021). b) Mann-Whitney test represents that Entropy$_{2.5}$ values was significantly higher (high heterogeneity) in tumors with core in peripheral than tumors with core in the center (P<0.001). c) Kruskal-Wallis test shows Entropy$_{2.5}$ values were significantly different among the number of irregular layers (P<0.001).

Inter-correlation among the visual assessment

Existence of cold defect (P=0.0001) and location of hottest core (P<0.0001) were associated with the number of irregular layers. Additionally, a significant inter-correlation between the existence of cold defect and location of hottest core was observed using Fisher's exact test (P=0.0024) (Table 3) (Figure 5).

Correlation between MTV and parameters of TH

In the analysis of the correlation between MTV and parameters of TH, MTV was correlated with AUC-CSH (P=0.0018), $Entropy_{PHL}$ (P<0.0001), $Entropy_{2.5}$ (P<0.0001), existence of cold defect (P=0.0001), location of hottest core (P<0.0001), and the number of irregular layers (P<0.0001) (Table 4).

Table 2. *Results of Kruskal-Wallis and Mann-Whitney tests for correlation between visual assessment by PHL method and indices of texture and intensity histogram analysis.*

	Cold defect[a]	Location of hottest core[a]	Number of irregular layers[b]
	Existence Vs non-existence	Center Vs periphery	
AUC-CSH	U=101.00, Z=2.83, **P=0.004***	U=339.50, Z=2.29, **P=0.021***	H=20.09, **P=0.002***
$Entropy_{PHL}$	U=160.00, Z=-1.69, **P=0.091**	U=245.50, Z=-3.55, **P<0.001***	H=31.15, **P<0.001***
$Entropy_{2.5}$	U=128.50, Z-2.29, **P=0.021***	U=204.50, Z=-4.11, **P<0.001***	H=33.56, **P<0.001***

*[a]Mann-Whitney test was used; [b]Kruskal-Wallis test was used, Italicized entries indicate * P<0.05*

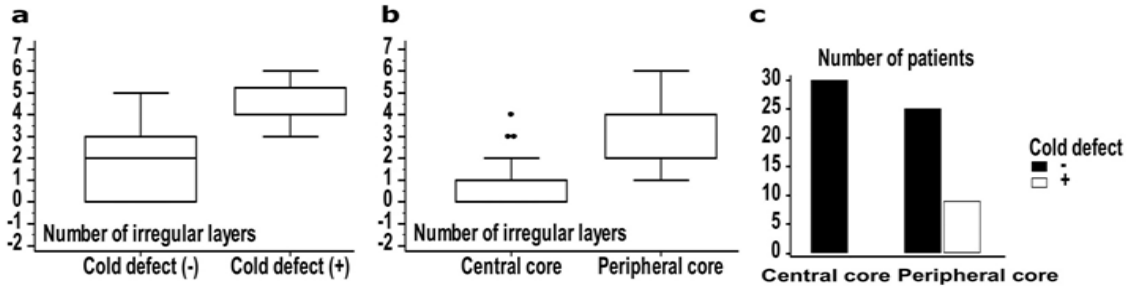

Figure 5. Inter-correlation among the visual assessments. a) Existence of cold defect showed the association with the number of irregular layers (P<0.001). b) Location of hottest core showed the association with the number of irregular layers (P<0.001). c) Fisher's exact test presented significant inter-correlation existence of cold defect and location of hottest core (P=0.002).

Table 3. *Inter-correlation among variables.*

Variables	Cold defect	Location of hottest core	Number of irregular layers
Cold defect	-		
Location of hottest core	P=0.002[a*]	-	
Number of irregular layers	P<0.001[b*]	P<0.001[b*]	-

*[a]Fisher's exact test was used; [b]Mann-Whitney test was used. Italicized entries indicate * P<0.05*

Table 4. *Correlation between MTV and parameters of heterogeneity.*

Variables	Cold defect[a]	Location of hottest core[a]	Number of irregular layers[b]	AUC-CSH[c]	$Entropy_{PHL}$[c]	$Entropy_{2.5}$[c]
MTV	U=51.00, Z=-3.79, **P<0.001***	U=98.00, Z=-5.54, **P<0.001***	H=47.00, **P<0.001***	ρ= -0.38 **P=0.001***	ρ= 0.63 **P<0.001***	ρ=0.65 **P<0.001***

*[a]Mann-Whitney test was used; [b]Kruskal-Wallis test was used; [c]Spearman rank correlation, Italicized entries indicate * P<0.05*

Discussion

In this study, we were able to provide a new visual assessment criterion of TH using the PHL method. The weaknesses of the existing visual assessment (visual scoring system) with low inter-observer agreements can be addressed by implementing the PHL method.

Fluorine-18-FDG PET/CT is a promising tool for non-invasive evaluation of TH [3, 4]. Different quantitative methods have been presented and analyses using texture metrics or intensity histogram metrics have been widely accepted [3, 6, 7]. Several studies have shown a significant correlation between visual assessment of TH and metrics analysis including texture and intensity histogram [8, 9]. Visual assessment, on the other hand, causes inter-observer disagreements. Recently, Jun et al. (2015, 2018) proposed a new reliable tumor segmentation method (PHL method) [11, 12]. They presented visual patterns to evaluate TH: The existence of cold defect, the location of hottest core, and number of irregular layers [11]. They observed relatively frequent emergence of cold defects, eccentric location of the hottest core of the tumor, and multiple irregular layers in heterogeneous tumors. The purpose of this study was to investigate whether the new visual patterns by the PHL method correlate with the TH analysis using texture or intensity histogram metrics. Furthermore, we evaluated whether three visual patterns were inter-correlated and whether tumor volume correlated with the parameters of TH.

Among the various methods for TH analysis, first-order entropy was extracted from texture metrics, and the AUC-CSH method was used for a correlative study. Entropy and AUC-CSH are widely studied parameters that have been proven to be useful and reliable for evaluation of TH [7, 14-16], prognosis in various cancers including lung cancer [17-20], and tumor differentiation studies [8, 21]. Each of the three visual patterns showed significant associations with entropy ($Entropy_{PHL}$ and $Entropy_{2.5}$) and AUC-CSH values. Although the association between the existence of cold defect and $Entropy_{PHL}$ (P=0.0911) was week, the existence of cold defect was significantly correlated with $Entropy_{2.5}$ (P= 0.0215). This might have been due to the differences in values according to the segmentation method (tumor threshold by PHL method versus fixed threshold of SUV [which was 2.5]). Additional prospective studies with a larger number of samples are needed to address this limitation.

Two additional results were identified in this study. First, a significant inter-correlation among the visual patterns of TH was observed with a strong inter-observer agreement (κ_w> 0.81). This may suggest that visual assessment using the PHL method is a reliable and useful method for evaluating TH in lung cancer. Second, all parameters for TH and tumor volume (MTV) were correlated, therefore indicating the larger tumors exhibit a wider range of heterogeneity than the smaller tumors. This result was similar to those reported in previous studies [22, 23]. Furthermore, this result was due to the fact that larger tumors have more potential to be composed of different types of cells, such as progressive cancer cells, and exhibit different conditions, such as tumor hypoxia. This region may represent various uptakes that can be described by ^{18}F-FDG PET/CT [24-26].

Several drawbacks limited this retrospective study. First, there were a limited number of subjects, and thus a larger cohort is needed to validate our results. Second, although the metrics and analyses (entropy and AUC-CSH) that were used for TH have been previously validated, they can also be affected by numerous factors, such as image acquisition, reconstruction, and processing [23]. Analysis based on PET images following a standardized protocol will be necessary in the future.

Despite limitations, the novelty of this study is as follows: (1) A new visual assessment to evaluate TH was presented. (2) Visual assessment through the PHL method shows a high inter-observer agreement unlike the existing visual scoring system. (3) A method that was simpler than texture and intensity histogram analysis was proposed. (4) A 10-step color scale was implemented, making easier to analyze the visual patterns.

In conclusion, the present study demonstrated a new visual assessment method with a high inter-observer agreement for evaluating TH. The visual assessment using the PHL method could be used as a potential marker for evaluating heterogeneous tumors beyond the capabilities of existing visual interpretation methods.

The authors declare that they have no conflicts of interest.

Bibliography

1. O'Sullivan F, Roy S, Eary J. A statistical measure of tissue heterogeneity with application to 3D PET sarcoma data. *Biostatistics* 2003; 4: 433-48.
2. O'Connor JP, Rose CJ, Waterton JC et al. Imaging intratumor heterogeneity: role in therapy response, resistance, and clinical outcome. *Clin Cancer Res* 2015; 21: 249-57.
3. Chicklore S, Goh V, Siddique M et al. Quantifying tumour heterogeneity in ^{18}F-FDG PET/CT imaging by texture analysis. *Eur J Nucl Med Mol Imaging* 2013; 40: 133-40.
4. Davnall F, Yip CS, Ljungqvist G et al. Assessment of tumor heterogeneity: an emerging imaging tool for clinical practice? *Insights Imaging* 2012; 3: 573-89.
5. Weber WA, Schwaiger M, Avril N. Quantitative assessment of tumor metabolism using FDG-PET imaging. *Nucl Med Biol* 2000; 27: 683-7.
6. El Naqa I, Grigsby P, Apte A et al. Exploring feature-based approaches in PET images for predicting cancer treatment outcomes. *Pattern Recognit* 2009; 42: 1162-71.
7. van Velden FH, Cheebsumon P, Yaqub M et al. Evaluation of a cumulative SUV-volume histogram method for parameterizing heterogeneous intratumoural FDG uptake in non-small cell lung cancer PET studies. *Eur J Nucl Med Mol Imaging* 2011; 38: 1636-47.
8. Watabe T, Tatsumi M, Watabe H et al. Intratumoral heterogeneity of F-18 FDG uptake differentiates between gastrointestinal stromal tumors and abdominal malignant lymphomas on PET/CT. *Ann Nucl Med* 2012; 26: 222-7.
9. Tixier F, Hatt M, Valla C et al. Visual versus quantitative assessment of intratumor ^{18}F-FDG PET uptake heterogeneity: prognostic value in non-small cell lung cancer. *J Nucl Med* 2014; 55: 1235-41.
10. Ren Y, Liu J, Wang L et al. Multiple metabolic parameters and visual assessment of ^{18}F-FDG uptake heterogeneity of PET/CT in advanced gastric cancer and primary gastric lymphoma. *Abdom Radiol (NY)*. 2020.
11. Jun S, Park JG, Seo Y. Accurate FDG PET tumor segmentation using the peritumoral halo layer method: a study in patients with esophageal squamous cell carcinoma. *Cancer Imaging* 2018; 18: 35.

12. Jun S, Kim H, Nam HY. A new method for segmentation of FDG PET metabolic tumour volume using the peritumoural halo layer and a 10-step colour scale. A study in patients with papillary thyroid carcinoma. *Nuklearmedizin* 2015; 54: 272-85.
13. Mena E, Sheikhbahaei S, Taghipour M et al. ^{18}F-FDG PET/CT Metabolic Tumor Volume and Intratumoral Heterogeneity in Pancreatic Adenocarcinomas: Impact of Dual-Time Point and Segmentation Methods. *Clin Nucl Med* 2017; 42: e16-e21.
14. Forgacs A, Pall Jonsson H, Dahlbom M et al. A Study on the Basic Criteria for Selecting Heterogeneity Parameters of ^{18}F-FDG PET Images. *PLoS One* 2016; 11: e0164113.
15. Galavis PE, Hollensen C, Jallow N et al. Variability of textural features in FDG PET images due to different acquisition modes and reconstruction parameters. *Acta Oncol* 2010; 49: 1012-6.
16. Yan J, Chu-Shern JL, Loi HY et al. Impact of Image Reconstruction Settings on Texture Features in ^{18}F-FDG PET. *J Nucl Med* 2015; 56: 1667-73.
17. Cook GJ, O'Brien ME, Siddique M et al. Non-Small Cell Lung Cancer Treated with Erlotinib: Heterogeneity of ^{18}F-FDG Uptake at PET-Association with Treatment Response and Prognosis. *Radiology* 2015; 276: 883-93.
18. Hyun SH, Kim HS, Choi SH et al. Intratumoral heterogeneity of ^{18}F-FDG uptake predicts survival in patients with pancreatic ductal adenocarcinoma. *Eur J Nucl Med Mol Imaging* 2016; 43: 1461-8.
19. Dong X, Sun X, Zhao X et al. The impact of intratumoral metabolic heterogeneity on postoperative recurrence and survival in resectable esophageal squamous cell carcinoma. *Oncotarget* 2017; 8: 14969-77.
20. Dong X, Sun X, Sun L et al. Early Change in Metabolic Tumor Heterogeneity during Chemoradiotherapy and Its Prognostic Value for Patients with Locally Advanced Non-Small Cell Lung Cancer. *PLoS One* 2016; 11: e0157836.
21. Nakajo M, Nakajo M, Jinguji M et al. The value of intratumoral heterogeneity of ^{18}F-FDG uptake to differentiate between primary benign and malignant musculoskeletal tumours on PET/CT. *Br J Radiol* 2015; 88: 20150552.
22. Larson SM, Erdi Y, Akhurst T et al. Tumor Treatment Response Based on Visual and Quantitative Changes in Global Tumor Glycolysis Using PET-FDG Imaging. The Visual Response Score and the Change in Total Lesion Glycolysis. *Clin Positron Imaging* 1999; 2: 159-71.
23. Hatt M, Tixier F, Pierce L et al. Characterization of PET/CT images using texture analysis: the past, the present... any future? *Eur J Nucl Med Mol Imaging* 2017; 44: 151-65.
24. Zhao S, Kuge Y, Mochizuki T et al. Biologic correlates of intratumoral heterogeneity in ^{18}F-FDG distribution with regional expression of glucose transporters and hexokinase-II in experimental tumor. *J Nucl Med* 2005; 46: 675-82.
25. Pugachev A, Ruan S, Carlin S et al. Dependence of FDG uptake on tumor microenvironment. *Int J Radiat Oncol Biol Phys* 2005; 62: 545-53.
26. Hockel M, Schlenger K, Aral B et al. Association between tumor hypoxia and malignant progression in advanced cancer of the uterine cervix. *Cancer Res* 1996; 56: 4509-15.